Editorial

Potential diverse applications of diffusion-derived vessel density (DDVD) pixel-by-pixel mapping

Dian-Qi Yao[1], Cun-Jing Zheng[2], Ying-Ying Deng[3], Bao-Lan Lu[4], Tao Lu[5], Gen-Wen Hu[6], Xin-Ming Li[7], Ben-Heng Xiao[1], Fu-Zhao Ma[1], Akmal Sabarudin[8], Ann D. King[1], Yì Xiáng J. Wáng[1]^

[1]Department of Imaging and Interventional Radiology, Faculty of Medicine, The Chinese University of Hong Kong, Hong Kong SAR, China; [2]Department of Radiology, Sun Yat-sen Memorial Hospital, Sun Yat-sen University, Guangzhou, China; [3]Department of Radiology, Shenzhen Yantian District People's Hospital, Shenzhen, China; [4]Department of Radiology, The First Affiliated Hospital, Sun Yat-sen University, Guangzhou, China; [5]Department of Radiology, Sichuan Provincial People's Hospital, University of Electronic Science and Technology of China, Chengdu, China; [6]Department of Radiology, Shenzhen People's Hospital (The Second Clinical Medical College, Jinan University, The First Affiliated Hospital, Southern University of Science and Technology), Shenzhen, China; [7]Department of Radiology, Zhujiang Hospital, Southern Medical University, Guangzhou, China; [8]Diagnostic Imaging and Radiotherapy Program, Faculty of Health Sciences, The National University of Malaysia, Kuala Lumpur, Malaysia

Correspondence to: Yì Xiáng J. Wáng, PhD. Department of Imaging and Interventional Radiology, Faculty of Medicine, The Chinese University of Hong Kong, 30-32 Ngan Shing Street, Shatin, New Territories, Hong Kong SAR, China. Email: yixiang_wang@cuhk.edu.hk.

Keywords: Diffusion-weighted imaging (DW imaging); diffusion-derived vessel density (DDVD); oncology; fibrosis; placenta accreta

Submitted Jan 25, 2024. Accepted for publication Feb 01, 2024. Published online Feb 20, 2024.
doi: 10.21037/qims-24-164
View this article at: https://dx.doi.org/10.21037/qims-24-164

On diffusion-weighted (DW) imaging, blood vessels show high signal when there is no diffusion gradient (b=0 s/mm^2), while they show low signal even when very low b-values (such as b=1 or 2 s/mm^2) are applied. Thus, the signal difference between images when the diffusion gradient is off and images when the diffusion gradient is on reflects the extent of tissue vessel density. Recently, Wáng (1) proposed that liver tissue micro-perfusion can be measured by a DW imaging-derived surrogate biomarker [diffusion-derived vessel density (DDVD)]:

$$\mathrm{DDVD}(\mathrm{b0b2}) = \frac{\mathrm{Sb0}}{\mathrm{ROIarea0}} - \frac{\mathrm{Sb2}}{\mathrm{ROIarea2}} \left[\text{arbitrary unit (au)/pixel}\right] \quad [1]$$

where ROIarea0 and ROIarea2 refer to the number of pixel in the selected region-of-interest (ROI) on b=0 s/mm^2 and b=2 s/mm^2 images, respectively. Sb0 refers to the measured total liver signal intensity within the ROI when b=0 s/mm^2, and Sb2 refers to the measured total liver signal intensity within the ROI when b=2 s/mm^2, thus Sb/ROIarea equates to the mean signal intensity within the ROI. Sb2 and ROIarea2 can also be approximated by other low b-value diffusion image's data. DDVD can be interpreted as a physiological surrogate of the area of micro-vessels per unit tissue area, which can be conceptually converted to a surrogate of the volume of micro-vessels per tissue unit volume if multiple slices are integrated.

The potential of clinical application of DDVD as a straightforward diffusion imaging biomarker has been recently demonstrated (1-6) (*Figure 1*). DDVD was initially proposed to evaluate the perfusion status of liver fibrosis, and it has shown that it is a useful parameter for the distinguishing of livers with and without fibrosis, and that livers with severer fibrosis tend to have even lower DDVD measurements than those with milder liver fibrosis (1-3). DDVD has also been tested in a number of other clinical scenarios (4-7). Zheng *et al.* (4) described spleen DDVD is decreased in viral hepatitis-b liver fibrosis patients. Huang *et al.* (5) showed that DDVD analysis demonstrates liver parenchyma has an age-dependent

^ ORCID: 0000-0001-5697-0717.

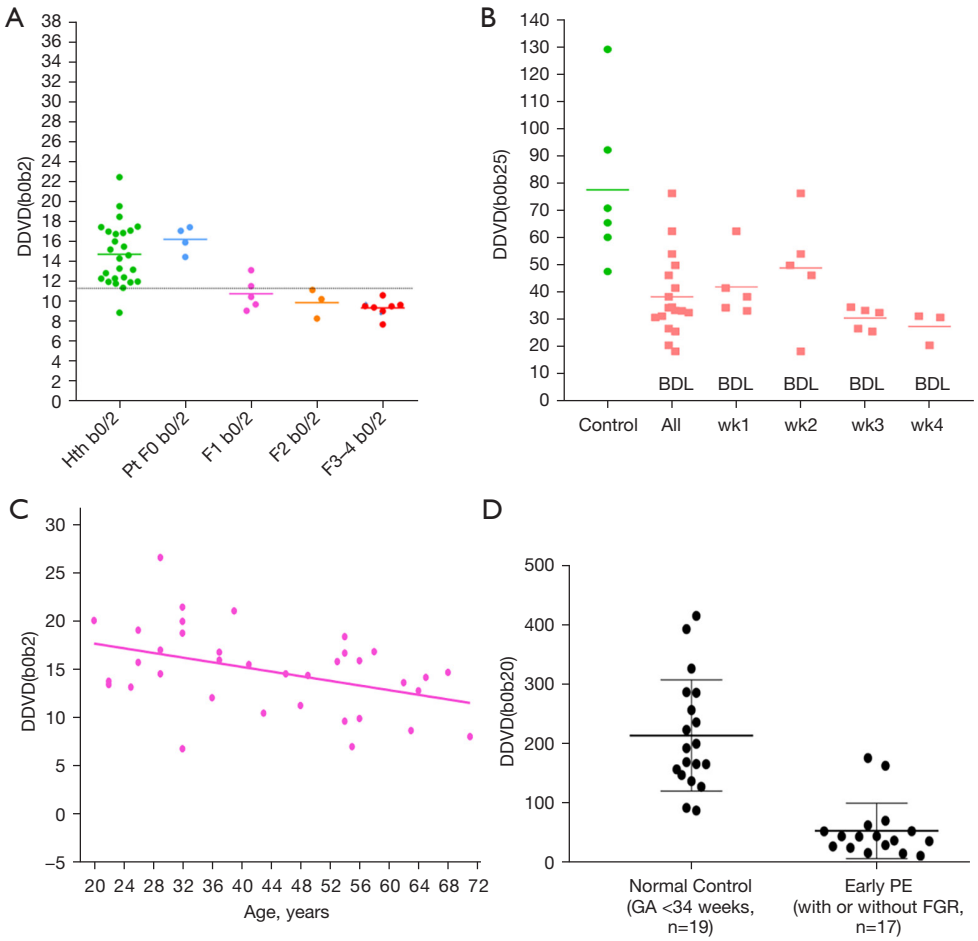

Figure 1 Examples of DDVD in tissue characterization. (A) Compared with healthy livers, lower DDVD value is noted for fibrotic livers (Hth b0/2: healthy volunteers. Pt F0 b0/2: patients with biopsy histology confirmed without liver fibrosis. F1, b0/2: cases of viral hepatitis type-B caused stage-1 liver fibrosis; F2, b0/2: cases of viral hepatitis type-B caused stage-2 liver fibrosis; F3-4, b0/2: cases of viral hepatitis type-B caused stage-3 and stage-4 liver fibrosis). DDVD(b0b2) is computed from b=0 and b=2 s/mm^2 DW images. (B) Rat livers with BDL show lower DDVD than healthy control rat livers. All: all BDL rats. wk1: rats of 1 week after BDL. wk2: rats of 2 weeks after BDL. wk3: rats of 3 weeks after BDL. wk4: rats of 4 weeks after BDL. DDVD(b0b25) is computed from b=0 and b=25 s/mm^2 DW images. (C) Aged-related liver perfusion reduction, as shown with DDVD, among healthy women. (D) Placenta with early PE show lower DDVD than normal control placenta. DDVD(b0b20) is computed from b=0 and b=20 s/mm^2 DW images. (A-D) are reused with permission from the studies (2,3,5,6), respectively. DDVD, diffusion-derived vessel density; BDL, biliary duct ligation; GA, gestational age; PE, preeclampsia; FGR, fetal growth restriction; DW, diffusion weighted.

decrease of micro-perfusion. This agrees with the known physiological age-dependent reduction in liver blood flow which has been well documented using a variety of technical methods including histology, dye dilution, and indicator clearance. He *et al.* (6) reported that DDVD analysis of the placenta allowed excellent separation of normal and early preeclampsia pregnancies. In a pilot study of 72 hepatocellular carcinoma (HCC) patients, the median ratio of tumor DDVD to adjacent liver DDVD was 2.94, which agrees with contrast agent dynamically enhanced computed tomography/magnetic resonance imaging (CT/MRI) data (7). Mean DDVD value was higher for HCCs with micro-vessel invasion (MVI) than HCCs without MVI, and mean DDVD value was higher for more malignment Edmondson-Steiner grade III or IV HCCs than for better differentiated Edmondson-Steiner grade I or II HCCs (7).

Compared with existing perfusion imaging techniques, DDVD protocol has many advantages. Compared with

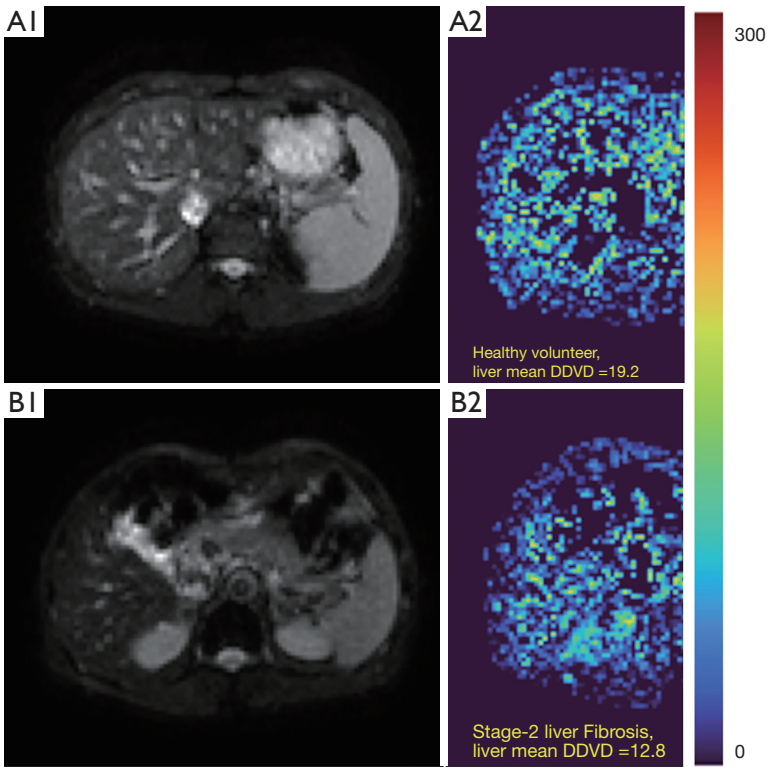

Figure 2 A case of normal liver (A) and a case of viral hepatitis type-B caused stage-2 liver fibrosis (B). DDVD map is computed from b=0 and b=2 s/mm^2 DW images. The fibrotic liver shows lower DDVD signal, thus lower blood perfusion, than the case of normal liver. (A1 and B1) b=0 s/mm^2 DW image. (A2 and B2) right liver DDVD map after the removal of vessel pixels [see description in the study (2)]. These two cases' materials are from reference (2). DDVD, diffusion-derived vessel density; DW, diffusion weighted.

contrast agent dynamically enhanced imaging, DDVD protocol does not involve contrast injection, data acquisition is much faster, and data post-processing is also relatively straightforward. Compared with contrast agent enhanced CT perfusion examination, DDVD is without radiation. Compared with contrast agent enhanced MRI perfusion examination, our initial experience suggests that DDVD measure is more stable. The analysis of DDVD requires only 2 b-values (with one being b=0 s/mm^2), allowing a short scanning time that can be completed within a single breath-hold duration, rendering it useful when the target organ is subject to respiratory motion. Intravoxel incoherent motion (IVIM) is also a noninvasive imaging method (but with a long scan time). However, it has been shown when there is T2 relaxation elevation of tumor (or other pathological tissue) relative to native tissue, standard IVIM modeling leads to suppression of perfusion fraction (and maybe also Dfast) measurement (8,9). The spleen is known to have similar total blood perfusion per unit volume to that of the liver. However, due to the longer T2 of the spleen relative to the T2 of the liver, IVIM analysis showed that spleen perfusion fraction is only half of that of the liver (10). On the other hand, T2 shortening leads to artificial elevation of perfusion fraction and Dfast measurement (11). Jerome *et al.* proposed a T2 extend IVIM model to correct this phenomenon, but this approach requires IVIM data acquisition to be run multiple times with varying TEs (12,13). This would lead to excessively long data acquisition in clinical settings.

As absolute magnetic resonance (MR) signal intensity is influenced by various factors, including B0/B1 spatial inhomogeneity, coil loading, receiver gain, etc., we have used the ratio of a lesion to its adjacent native tissue (such as the ratio of HCC's DDVD to liver DDVD) to minimize these scaling factors (7). Following this, it may be useful to present pixel-by-pixel map of DDVD, so that the difference between the DDVD of a diseased tissue and DDVD of native/adjacent tissues can be compared visually. In this article, we present some examples of such DDVD map (*Figures 2-12*). We try to convey the message that DDVD map can be applied in multiple organs and multiple

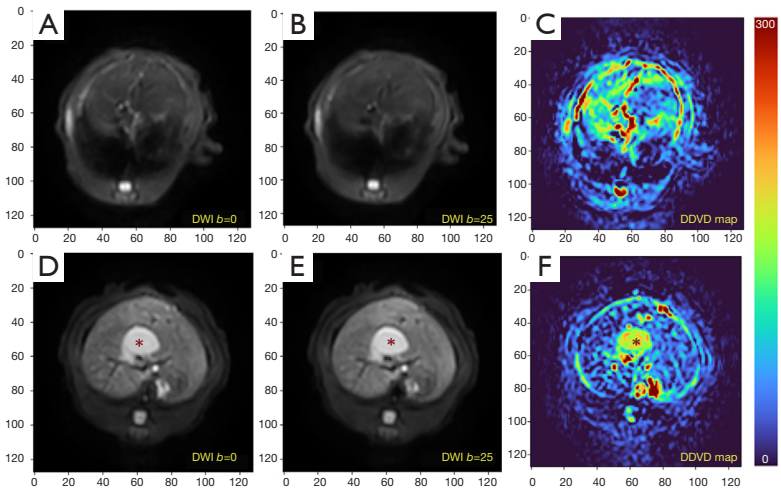

Figure 3 Liver DDVD maps of a control rat and a rat of 4 weeks after BDL. DW imaging included b=0 and b=25 s/mm^2 images [(A-C) control rat; (D-F) BDL rat]. DDVD map is computed from b=0 and b=25 s/mm^2 DW images. DDVD maps show higher liver parenchyma value for the control rat [(C) 58.2 arbitrary unit/pixel] than for the BDL rat [(F) 27.8 arbitrary unit/pixel]. Lower DDVD in the BDL rat liver is considered due to lower blood perfusion associated with liver fibrosis. A few artefacts are noted on DDVD map. In (C and F), the peripheral high signal rims around the liver are caused by misalignment between b=0 and b=25 s/mm^2 images, which is likely caused by respiration motion. Dilated biliary duct (*) also shows high signal on (F). Dilated biliary duct is without blood perfusion. The dilated biliary duct's falsely high DDVD value and also the CSF DDVD values are considered to be due to T2 effect. According to the initial definition of DDVD, the second b-value should be very low so to eliminate the T2 effect (1). For this rat study, since the second b-value was 25 s/mm^2, then T2 effect is introduced for tissues/structures with long T2 leading to high value on DDVD map (see explanation in *Figure 4*). The rat materials are from reference (3). DWI, diffusion-weighted imaging; DDVD, diffusion-derived vessel density; BDL, biliary duct ligation; DW, diffusion weighted; CSF, cerebrospinal fluid.

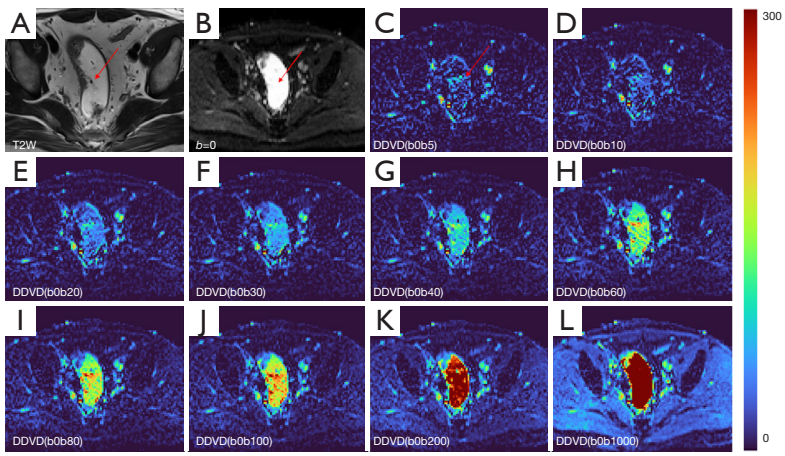

Figure 4 The impact of T2 relaxation time on DDVD map calculation. (A,B) T2 weighted image and b=0 s/mm^2 DW image respectively, with the fluid in the sigmoid (arrow) showing high signal due to its long T2. DDVD(b0b5) map is computed from b=0 and b=5 s/mm^2 DW images, and DDVD(b0b10) map is computed from b=0 and b=10 s/mm^2 DW images. (C,D) DDVD(b0b5) and DDVD(b0b10) maps show the fluid in the sigmoid is low signal. (K,L) DDVD(b0b200) and DDVD(b0b1000) maps show the fluid in the sigmoid is very high signal due to its long T2. (E) DDVD(b0b20) map; (F) DDVD(b0b30) map; (G) DDVD(b0b40) map; (H) DDVD(b0b60) map; (I) DDVD(b0b80) map; (J) DDVD(b0b100) map. From DDVD(b0b20) to DDVD(b0b1000), the fluid in the sigmoid shows increasingly higher signal on DDVD map. Commonly, when the second b-value is less than 10 s/mm^2, the T2 effect of a tissue or a substance is not apparent on DDVD map, while after second b-value is more than 10 s/mm^2, the T2 effect of a tissue or a substance is visible on DDVD map. Therefore, we advocate the second b-value for DDVD calculation should be small (1). T2W, T2 weighted; DDVD, diffusion-derived vessel density; DW, diffusion weighted.

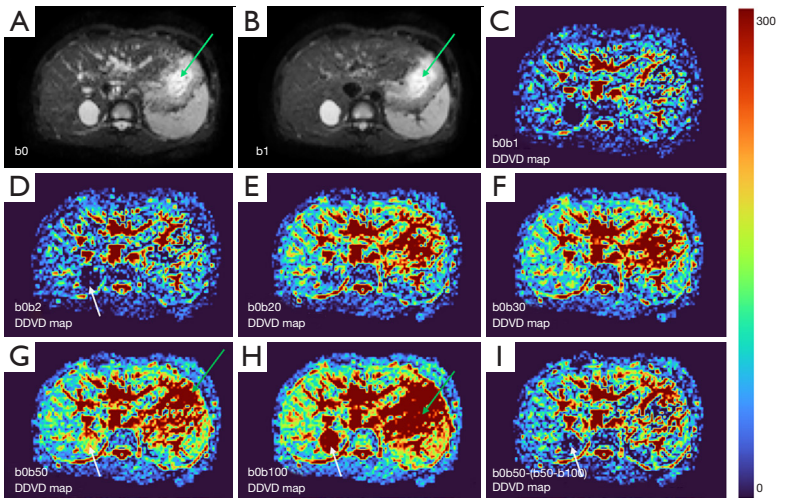

Figure 5 Appearance of a hepatic cyst (white arrow) on DDVD map. DDVD(b0b1) map (C) is computed from b=0 and b=1 s/mm^2 DW images, and DDVD(b0b2) map (D) is computed from b=0 and b=2 s/mm^2 DW images. On DDVD(b0b1) map and DDVD(b0b2) map, the hepatic cyst shows very low signal, consistent with that hepatic cyst has no perfusion. Due to the long T2 of hepatic cyst, hepatic cyst shows iso- signal to adjacent liver on DDVD(b0b30) map, higher signal compared with the adjacent liver on DDVD(b0b50) map and DDVD(b0b100) map. On the DDVD map (I) entitled 'b0b50-(b50-b100)', [i.e., (signal at b0 – signal at b50) – (signal at b50 – signal at b100), hereby 'signal at b0' refers to signal intensity on b=0 s/mm^2 DW image], we aim to minimise the diffusion effect while maintaining the perfusion effect. We assume that, approximately diffusion effect (b0-b50) = diffusion effect (b50-b100), while perfusion effect (b0-b50) >> perfusion effect (b50-b100). Green arrow denotes the signal due to fluid in the stomach. As the images in this case were acquired with respiratory gating (rather than breath-holding), the alignment of images of varying b-values are not perfect. (A) b=0 s/mm^2 DW image. (B) b=1 s/mm^2 DW image. (E) DDVD(b0b20) map; (F) DDVD(b0b30) map; (G) DDVD(b0b50) map; (H) DDVD(b0b100) map. DDVD, diffusion-derived vessel density; DW, diffusion weighted.

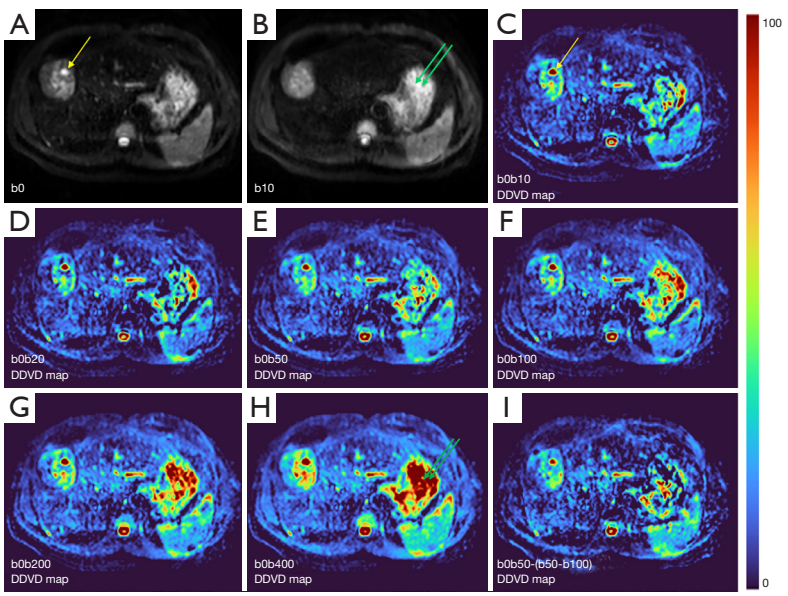

Figure 6 Appearance of a hepatocellular carcinoma on DDVD map. DDVD(b0b10) map (C) is computed from b=0 and b=10 s/mm^2 DW images, and DDVD(b0b20) map (D) is computed from b=0 and b=20 s/mm^2 DW images. On DDVD(b0b10) map, the hepatocellular carcinoma shows higher signal compared with the adjacent liver. The same as in *Figure 5*, on the DDVD map (I) entitled 'b0b50-(b50-b100)', [i.e., (signal at b0 – signal at b50) – (signal at b50 – signal at b100), hereby 'signal at b0' refers to signal intensity on b=0 s/mm^2 DW image], we aim to minimise the diffusion effect while maintaining the perfusion effect. We assume that, approximately diffusion effect (b0-b50) = diffusion effect (b50-b100),

while perfusion effect (b0-b50) >> perfusion effect (b50-b100). With *Figure 5*, the hepatic cyst shows low signal on DDVD map of 'b0b50-(b50-b100)'. The hepatocellular carcinoma remains higher signal compared with the adjacent liver on DDVD map of 'b0b50-(b50-b100)' in this figure. The yellow arrow denotes a focus of necrotic change which was imaged on b=0 s/mm^2 image while missed on b=10 s/mm^2 image (of this slice), and this also cause an artefact on subsequent DDVD maps. As the images in this case were acquired with free-breathing, the alignment of images of varying b-values is not perfect. Green arrows denote the signal due to fluid in the stomach. (A) b=0 s/mm^2 DW image. (B) b=10 s/mm^2 DW image. (E) DDVD(b0b50) map; (F) DDVD(b0b100) map; (G) DDVD(b0b200) map. (H) DDVD(b0b400) map. DDVD, diffusion-derived vessel density; DW, diffusion weighted.

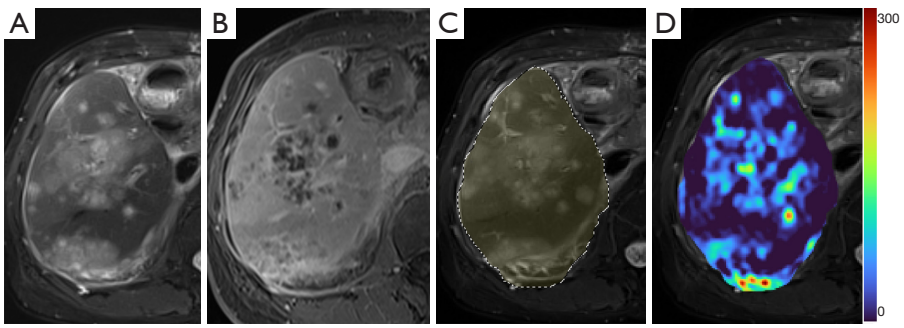

Figure 7 An example of DDVD map with liver region segmented and overlayed on b=0 s/mm^2 DW image. This patient had cholangiocarcinoma with metastasis and was under treatment. DDVD map is computed from b=0 and b=10 s/mm^2 images, showing multiple tumor sites with increased DDVD relative to the liver parenchyma and thus suggesting increased blood perfusion for the tumor nodules. (A) T2-weighted anatomical image; (B) gadolinium enhanced T1-weighted image; (C) b=0 s/mm^2 DW image with liver region segmented by a ROI (dashed circle); (D) DDVD map of the liver region is overlayed on b=0 s/mm^2 DW image. DDVD, diffusion-derived vessel density; DW, diffusion weighted; ROI, region-of-interest.

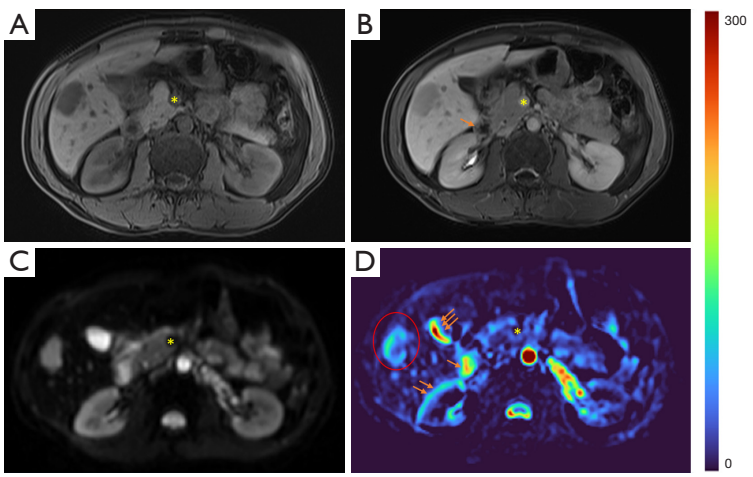

Figure 8 An example of liver DDVD map with a metastatic tumor from nasopharyngeal carcinoma. DDVD map is computed from b=0 and b=10 s/mm^2 DW images. Tumor (red circle) appears higher perfusion relative to adjacent liver. (A) T1-weighted anatomical image; (B) gadolinium enhanced T1-weighted image; (C) b=0 s/mm^2 DW image; (D) DDVD map. *, superior mesenteric artery shows flow-related signal void on DW image (C) and DDVD map (D). Single arrow denotes duodenum showing high signal on DDVD map which is caused by the fluid in the lumen and duodenum peristalsis during the DW imaging. This is a common artifact of gastrointestinal tract. Double arrows for right kidney border and triple arrows for gallbladder denote artifacts due to misalignment between b=0 and b=10 s/mm^2 images. Note that right renal veins are well shown with high value on DDVD map. CSF commonly shows high value on DDVD map. DDVD, diffusion-derived vessel density; DW, diffusion weighted; CSF, cerebrospinal fluid.

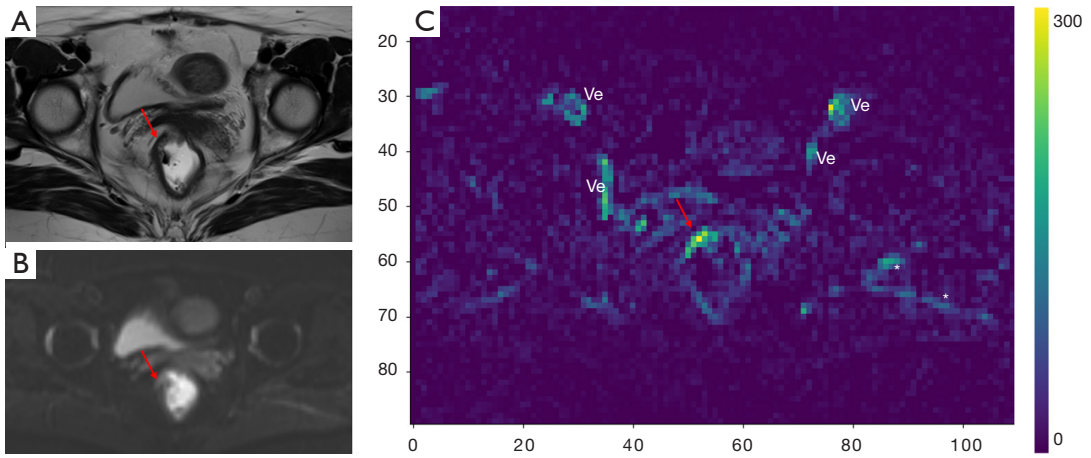

Figure 9 An example of DDVD map showing a hyper-vascular rectal carcinoma (arrow). DDVD map is computed from b=0 and b=5 s/mm^2 DW images. (A) T2-weighted anatomical image; (B) b=0 s/mm^2 DW image; (C) DDVD map. *, artefacts due to fatty fascia misalignment between b=0 and b=5 s/mm^2 images. Ve, vessels; DDVD, diffusion-derived vessel density; DW, diffusion weighted.

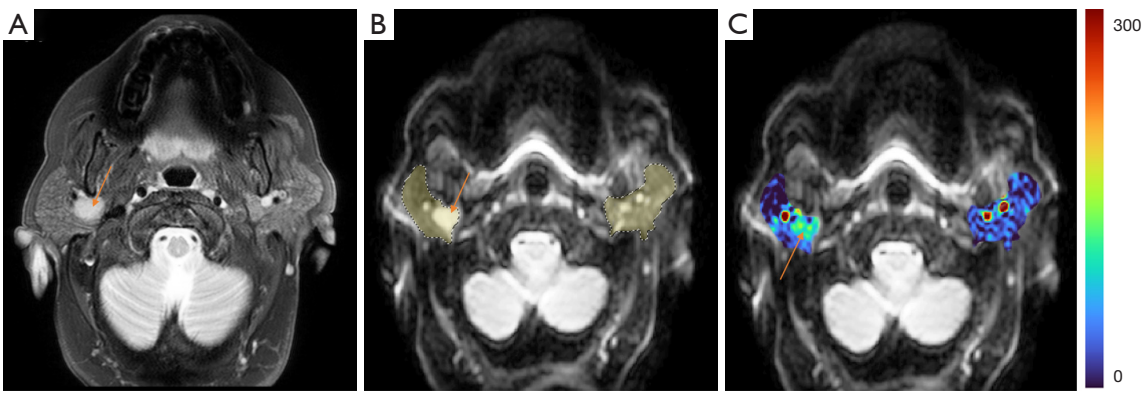

Figure 10 A case of right parotid gland malignant tumor (arrow) with bilateral parotid gland segmented and overlayed on b=0 s/mm^2 DW image. DDVD map is computed from b=0 and b=20 s/mm^2 images. Tumor appears higher perfusion relative to adjacent parotid gland tissue. Note that vessels near the parotid gland show very high signal on DDVD map. (A) T2-weighted anatomical image; (B) b=0 s/mm^2 DW image with bilateral parotid glands and tumor segmented by ROIs (dashed circles); (C) DDVD maps of bilateral parotid glands and tumor are overlayed on b=0 s/mm^2 DW image. DDVD, diffusion-derived vessel density; DW, diffusion weighted; ROI, region-of-interest.

tissues, helping to evaluate different pathological entities particularly concerning their perfusion status. It has been shown apparent diffusion coefficient (ADC) measure is heavily affected by T2 effect (14,15); however, T2 effect can be minimized for DDVD when appropriate scan protocols or data processing protocols are adopted (*Figure 5*).

How to acquire DDVD scan protocol and how to conduct image postprocessing have not been optimized yet. Increasing number of excitations (NEX) can improve DDVD measure stability, and since the DDVD protocol is very fast, high NEX is feasible. *Figures 2-11* show that DDVD map should be viewed side-by-side with the source DW images. The clinical application potential of DDVD map will be further studied.

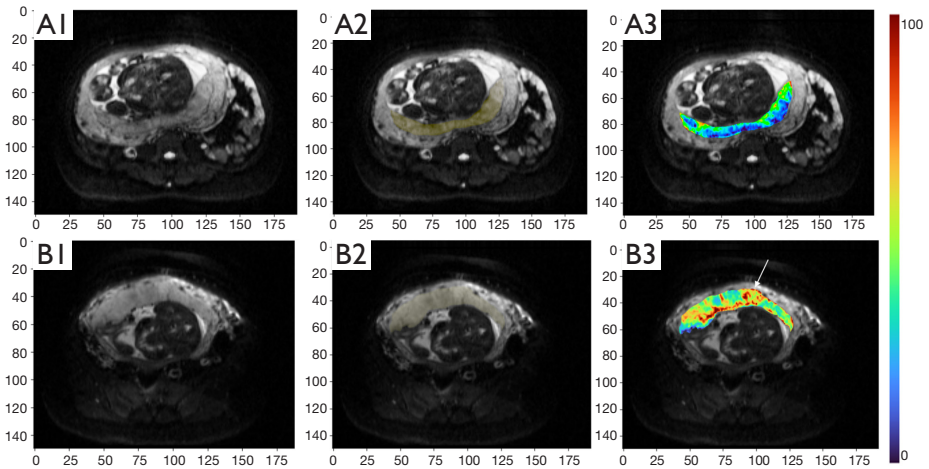

Figure 11 DDVD map, computed from b=0 and b=50 s/mm^2 images, of placenta percreta demonstrates higher blood perfusion. (A) Normal placenta; (B) placenta percreta. (A1) is a b=0 s/mm^2 DW image showing normal placenta. (A2) Placenta region in (A1) is segmented with a ROI. (A3) DDVD map of the placenta region is overlayed on b=0 s/mm^2 DW image, with ROI based on (A2). (B1) is a b=0 s/mm^2 DW image with placenta percreta. (B2) Placenta region in (B1) is segmented with a ROI. (B3) DDVD color map of the placenta region is overlayed on b=0 s/mm^2 DW image, with ROI based on (B2). Compared the case in (A3), the placenta in (B3) shows both general and focal (arrow) increased DDVD signal. DDVD, diffusion-derived vessel density; DW, diffusion weighted; ROI, region-of-interest.

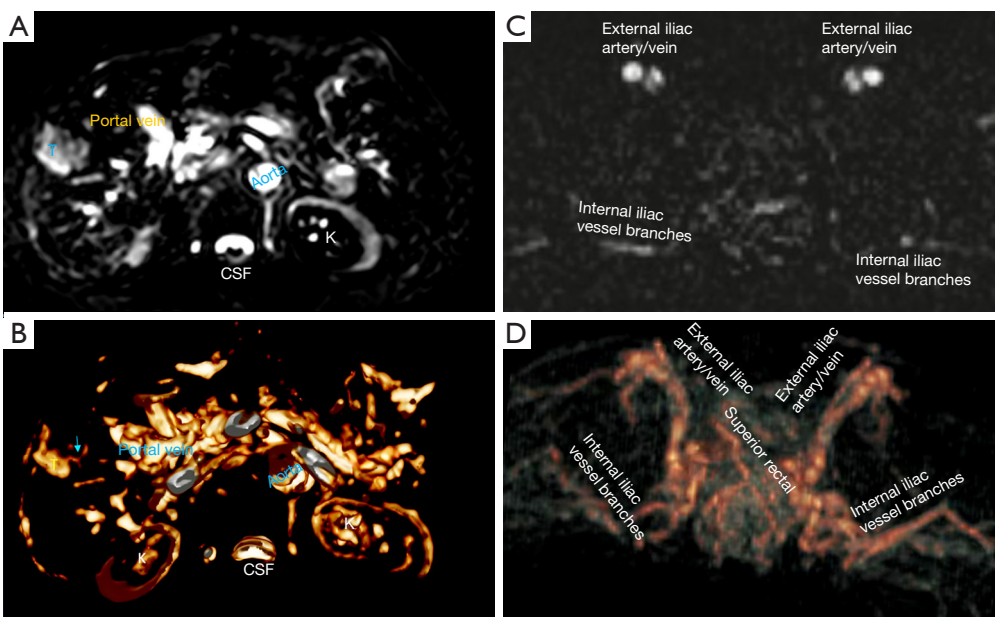

Figure 12 3D surface-rendering of DDVD map. (A) A DDVD map showing a hepatocellular carcinoma (T). DDVD map is computed from b=0 and b=2 s/mm^2 DW images. The filling defect in aorta is likely an artefact. The voxel size of the original DW imaging for (A) is 0.76×0.76×7 mm^3. (B) 3D surface-rendering of DDVD maps at the level of the hepatocellular carcinoma (T). Arrow in (B) denotes a vessel, possibly a vein. The visualization of mesenteric vessels in this image is contaminated by signal from bowels. (C) A DDVD map at the pelvis level. DDVD map is computed from b=0 and b=5 s/mm^2 DW images. The voxel size of the original DW imaging for (C) is 2.73×2.73×6.0 mm^3. (D) 3D surface-rendering of DDVD maps of the pelvis. This approach described here can in theory be used for angiography. The patient in (C,D) was scanned with the rectum extended with fluid. CSF, cerebrospinal fluid; K, kidney; 3D, three-dimensional; DDVD, diffusion-derived vessel density; DW, diffusion weighted.

Acknowledgments

Funding: This work was supported by Hong Kong GRF Project (No. 14112521).

Footnote

Provenance and Peer Review: This article was commissioned by the editorial office, *Quantitative Imaging in Medicine and Surgery*. The article did not undergo external peer review.

Conflicts of Interest: All authors have completed the ICMJE uniform disclosure form (available at https://qims.amegroups.com/article/view/10.21037/qims-24-164/coif). Y.X.J.W. serves as the Editor-in-Chief of *Quantitative Imaging in Medicine and Surgery*. Y.X.J.W. is the founder of Yingran Medicals Ltd., which develops medical image-based diagnostics software. The other authors have no conflicts of interest to declare.

Ethical Statement: The authors are accountable for all aspects of the work in ensuring that questions related to the accuracy or integrity of any part of the work are appropriately investigated and resolved.

References

1. Wáng YXJ. Living tissue intravoxel incoherent motion (IVIM) diffusion MR analysis without b=0 image: an example for liver fibrosis evaluation. Quant Imaging Med Surg 2019;9:127-33.
2. Xiao BH, Huang H, Wang LF, Qiu SW, Guo SW, Wáng YXJ. Diffusion MRI Derived per Area Vessel Density as a Surrogate Biomarker for Detecting Viral Hepatitis B-Induced Liver Fibrosis: A Proof-of-Concept Study. SLAS Technol 2020;25:474-83.
3. Hu GW, Zheng CJ, Zhong WX, Zhuang DP, Xiao BH, Wáng YXJ. Usefulness of diffusion derived vessel density computed from a simplified IVIM imaging protocol: An experimental study with rat biliary duct blockage induced liver fibrosis. Magn Reson Imaging 2021;84:115-23.
4. Zheng CJ, Huang H, Xiao BH, Li T, Wang W, Wáng YXJ. Spleen in viral Hepatitis-B liver fibrosis patients may have a reduced level of per unit micro-circulation: non-invasive diffusion MRI evidence with a surrogate marker. SLAS Technol 2022;27:187-94.
5. Huang H, Zheng CJ, Wang LF, Che-Nordin N, Wáng YXJ. Age and gender dependence of liver diffusion parameters and the possibility that intravoxel incoherent motion modeling of the perfusion component is constrained by the diffusion component. NMR Biomed 2021;34:e4449.
6. He J, Chen C, Xu L, Xiao B, Chen Z, Wen T, Wáng YXJ, Liu P. Diffusion-Derived Vessel Density Computed From a Simplified Intravoxel Incoherent Motion Imaging Protocol in Pregnancies Complicated by Early Preeclampsia: A Novel Biomarker of Placental Dysfunction. Hypertension 2023;80:1658-67.
7. Li XM, Yao DQ, Quan XY, Li M, Chen W, Wáng YXJ. Perfusion of hepatocellular carcinomas (HCC) measured by diffusion-derived vessel density (DDVD) biomarker: higher HCC perfusion than earlier IVIM reports. NMR Biomed 2024. doi: 10.1002/nbm.5125.
8. Ma FZ, Wáng YXJ. T(2) relaxation time elongation of hepatocellular carcinoma relative to native liver tissue leads to an underestimation of perfusion fraction measured by standard intravoxel incoherent motion magnetic resonance imaging. Quant Imaging Med Surg 2024;14:1316-22.
9. Wáng YXJ, Sabarudin A. Underestimation of liver hemangioma perfusion fraction by standard intravoxel incoherent motion diffusion magnetic resonance imaging. Quant Imaging Med Surg 2024;14:2128-35.
10. Yu WL, Xiao BH, Ma FZ, Zheng CJ, Tang SN, Wáng YXJ. Underestimation of the spleen perfusion fraction by intravoxel incoherent motion MRI. NMR Biomed 2023;36:e4987.
11. Xiao BH, Wáng YXJ. Different tissue types display different signal intensities on b = 0 images and the implications of this for intravoxel incoherent motion analysis: Examples from liver MRI. NMR Biomed 2021;34:e4522.
12. Lemke A, Laun FB, Simon D, Stieltjes B, Schad LR. An in vivo verification of the intravoxel incoherent motion effect in diffusion-weighted imaging of the abdomen. Magn Reson Med 2010;64:1580-5.
13. Jerome NP, d'Arcy JA, Feiweier T, Koh DM, Leach MO,

Collins DJ, Orton MR. Extended T2-IVIM model for correction of TE dependence of pseudo-diffusion volume fraction in clinical diffusion-weighted magnetic resonance imaging. Phys Med Biol 2016;61:N667-80.
14. Wáng YXJ, Zhao KX, Ma FZ, Xiao BH. The contribution of T2 relaxation time to MRI-derived apparent diffusion coefficient (ADC) quantification and its potential clinical implications. Quant Imaging Med Surg 2023;13:7410-6.
15. Wáng YXJ, Ma FZ. A tri-phasic relationship between T2 relaxation time and magnetic resonance imaging (MRI)-derived apparent diffusion coefficient (ADC). Quant Imaging Med Surg 2023;13:8873-80.

Cite this article as: Yao DQ, Zheng CJ, Deng YY, Lu BL, Lu T, Hu GW, Li XM, Xiao BH, Ma FZ, Sabarudin A, King AD, Wáng YXJ. Potential diverse applications of diffusion-derived vessel density (DDVD) pixel-by-pixel mapping. Quant Imaging Med Surg 2024;14(3):2136-2145. doi: 10.21037/qims-24-164

